ISSN No: -2456-2165 https://doi.org/10.38124/ijisrt/25oct786

A Study on Digital MTI Processors & Frequency Pulse

Mohammad Anisur Rahaman[1]; Ridoy Kumar Roy[2]; Syed Mohammed Daiam Ullah[3]; Sourav Roy[4]

[1]Information Technology Management, Asia Pacific University of Technology & Innovation (APU), Malaysia.
[2] Information & Communication Engineering, College of Information Science & Engineering, Hohai University, China
[3] Information & Communication Engineering, College of Information Science & Engineering, Hohai University, China
[4] Nanjing University of Posts & Telecommunications, Nanjing, China

Publication Date: 2025/10/30

Abstract: This research explores the optimization of moving target indication (MTI) systems in contemporary radar technology. We want to increase radar system performance by using improvements like step-scan antennas and digital signal processing. Despite these developments, obsolete CPU architecture prevents MTI systems from reaching their full potential. To overcome this, we present unique design techniques that are suitable for both staggered and unstaggered Pulse Repetition Frequency (PRF) setups. These techniques focus MTI performance while reducing processor response variances at various target speeds. Specialized processor designs, including techniques such as simplex approaches and simultaneous linear equation solving, are being developed to improve response uniformity, particularly in unstaggered PRF configurations. We hope to enable radar systems for a wide range of operating conditions by thoroughly investigating MTI concepts, tactics for minimizing obstacles such as the blind speed problem, and optimization methodologies

Keywords: *Adaptive Moving Target Indication (AMTI), MTI Processors, Blind Speeds, Staggered PRF, Unstaggered PRF, Doppler Frequency, Single Delay Line Canceller.*

How to Cite: Mohammad Anisur Rahaman; Ridoy Kumar Roy; Syed Mohammed Daiam Ullah; Sourav Roy (2025). A Study on Digital MTI Processors & Frequency Pulse. *International Journal of Innovative Science and Research Technology*, 10(10), 1820-1837. https://doi.org/10.38124/ijisrt/25oct786

I. INTRODUCTION

Radar systems have become crucial for modern surveillance, navigation, and defense applications, allowing the detection and tracking of objects over extensive distances across various environmental conditions (Skolnik, 2008). In contrast to optical or infrared sensors, radar functions effectively under adverse weather and low-visibility conditions, delivering precise range and velocity data. Radar detects aircraft, ships, motor vehicles, and natural phenomena such as rain and birds by transmitting electromagnetic waves and analyzing the echoes that return.

A significant challenge in radar operation is the differentiation of moving targets from stationary background reflections, referred to as clutter. The Moving Target Indication (MTI) technique employs Doppler-based filtering to distinguish between stationery and dynamic echoes. Traditional MTI filters frequently experience performance degradation because of blind speeds, nonstationary clutter, and hardware-induced interference (Richards, 2005; Nathanson, 1969). Modern radar systems increasingly utilize digital signal processing (DSP) and adaptive filtering techniques to improve target detection in complex environments (Tan & Jiang, 2025; Kuo, 2006).

Recent advancements in radar signal processing have led to the emergence of both adaptive and non-adaptive MTI systems, which effectively reduce clutter and interference under diverse operating conditions (Riabukha et al., 2022). The combination of space–time adaptive processing (STAP) and deep learning-based filtering has enhanced clutter suppression in maritime and airborne radar applications (Klemm, 2006; Cho et al., 2025). Advanced noise radar techniques and waveform optimization strategies enhance detection sensitivity and robustness (Galati et al., 2022; Gini, 2021).

Despite advancements, limitations in blind speed and residual cluster persistently challenge the performance of MTI

ISSN No: -2456-2165 https://doi.org/10.38124/ijisrt/25oct786

radar, especially in dynamic and congested operational environments. This study examines the optimization of MTI filter design utilizing adaptive signal processing and staggered pulse repetition frequency (PRF) techniques to enhance detection accuracy and minimize interference effects. This approach integrates theoretical modeling with MATLAB simulations to assess MTI performance under different clutter conditions, enhancing the reliability and adaptability of radar systems for future applications.

II. THEORETICAL BACKGROUND AND LITERATURE REVIEW

The first Moving Target Indication (MTI) radar systems were developed in the 1950s, using analog delay lines to isolate moving targets and cancel out stationary echoes. Early implementations faced limitations due to analog noise, restricted dynamic range, and the blind-speed problem, wherein targets moving at certain velocities generated Doppler shifts that were indistinguishable from stationary clutter (Nathanson, 1969; Kerr, 1965). MTI technology has become essential in airborne and ground-based surveillance, owing to its capability to identify low-velocity objects against static reflections, despite existing challenges.

The transition from analog to digital signal processing (DSP) has led to significant advancements in radar systems. Contemporary digital radars utilize sophisticated algorithms for adaptive clutter suppression, multi-pulse integration, and Doppler filtering (Richards, 2005; Tan & Jiang, 2025). These innovations have enhanced radar sensitivity and reliability across various operating conditions. Adaptive MTI and space-time adaptive processing (STAP) architectures are essential for managing nonstationary clutter and interference in high-density environments (Klemm, 2006; Vaidyanathan, 1990).

Recent studies emphasize the necessity of enhancing MTI performance for new radar applications. Riabukha et al. (2022) conducted an experimental comparison of adaptive and non-adaptive MTI systems across various radar frequency bands, revealing that adaptive processing markedly enhances clutter attenuation and target detectability. Cho et al. (2025) implemented adaptive sea-clutter suppression algorithms to improve detection capabilities in maritime radar systems utilized by uncrewed surface vehicles. Research on noise radar and waveform design has enhanced detection capabilities through improved range resolution and decreased mutual interference (Galati et al., 2022; Gini, 2021).

Residual clutter, dynamic interference, and Doppler ambiguities continue to pose significant challenges to MTI performance, despite recent advancements. Resolving these issues necessitates the integration of adaptive filtering, staggered pulse repetition frequency (PRF) design, and machine-learning-based signal processing techniques to enhance target discrimination and operational flexibility. This research proposes an enhanced MTI processor design that integrates theoretical modeling and simulation to assess performance improvements in radar data processing across different clutter and interference scenarios, building on recent developments (You et al., 2016; Xu et al., 2024).

- *MTI & Doppler Frequency Shift*

Radar designers faced ongoing issues in identifying target signals from interference caused by noise, neighboring radars, or environmental reflections such as trees, topography, and weather. Such traffic congestion can range up to 70 decibels, frequently overpowering weak targets and compromising performance. Reliable detection in these settings necessitates advanced signal processing and interference avoidance approaches to improve radar performance in complicated environments.

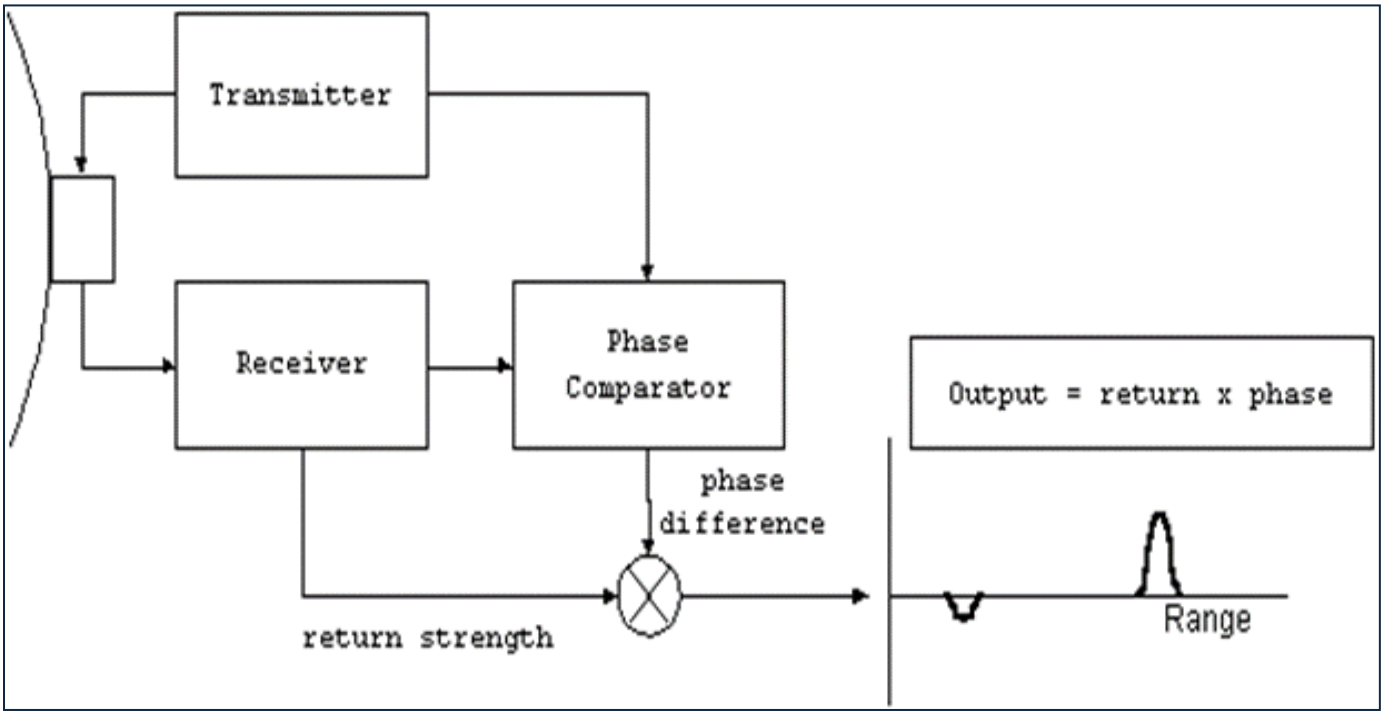

Fig 1 Phase Comparison Output

ISSN No: -2456-2165 https://doi.org/10.38124/ijisrt/25oct786

The transmitted and returning signal phases are compared to detect target motion. When the distance changes by half a wavelength, the phase comparator output changes as well, finishing a cycle. The Doppler effect explains this variance, which allows radar to differentiate moving targets from stationary clutter by using frequency changes.

MTI radar adopts low PRF, avoiding range but causing Doppler ambiguities; pulse-Doppler radar uses high PRF, reversing this trade-off.

Divide the distance (R) by calculating the total number of wavelengths (λ) in the radar's round-trip route to the target. If the distance (R) and wavelength (λ) are measured in the same units, this calculation provides the total angular excursion. To determine the total angular excursion, multiply the number of wavelengths by 2π radians. This relationship explains the angular displacement of the radar signal as it travels round-trip to and from the target.

$$\varphi = 2\pi * \frac{2R}{\lambda} = \frac{4\pi R}{\lambda} \text{radians} \dots\dots\dots\dots\dots\dots\dots\dots\dots\dots\dots\dots (1)$$

If the target is in motion relative to the Radar, R and the phase are continually changing.

The Doppler angular frequency ωd is given by

$$\omega d = 2\pi f_d = d\varphi/dt = d/dt(4\pi R/\lambda) = 4\pi/\lambda\ (dR/dt) = 4\pi v_r/\lambda \quad (2)$$

f_d = Doppler frequency shift

v_r= is relative (or radial) velocity of target with respect to radar

The Doppler frequency shift

$$f_d = 2vr/\lambda = 2vr\ (f_0/c) \dots\dots\dots\dots\dots\dots\dots\dots\dots\dots\dots\dots (3)$$

Applications for Doppler Frequency Shift

- CW radar detects moving targets and measures their radial velocity.
- Synthetic aperture radar and inverse synthetic aperture provide target images.
- Metrological radars are used to measure wind shear.

➢ *Extracts the Doppler Frequency Shifted Echo Signal*

$A_t \sin [2\pi f_t\ t$ [Transmitted Signal] …….. (4)

$A_r \sin [2\pi f_t\ (t - T_R)$ [Received Signal] …… (5)

$V_{recieve} = A_r \sin [2\pi f_t\ (t - T_R)$ [Received Signal] …… (6)

$V_{recieve} = A_r \sin [2\pi f_t\ (t - \frac{2R}{C})$ …….. (7)

$V_{recieve} = A_r \sin [2\pi f_t\ (t - \frac{2(R_0 - V_r t)}{C})$ …… (8)

If target is moving toward the radar, then Range changes to

$$R = (R_0 - V_r t)$$

$V_{recieve} = A_r \text{Sin} [2\pi f_t\ t\ (1 + \frac{2v_r}{c}) - \frac{4\pi f_t R_0}{C}]$ …….. (9)

The received signal is heterodyned with the reference signal

$A_{ref} \text{Sin} 2\pi f_t t$ and and the difference frequency is recovered, represented as

$$V_d = A_d \text{COS}\left(2\pi f_d t - \frac{4\pi R_0}{\lambda}\right) \dots\dots\dots\dots\dots\dots (10)$$

MTI and pulse-Doppler radars confront a first blind speed, in which Doppler shifts correspond to half-wavelength changes, resulting in phase cancellation and preventing accurate velocity detection beyond maximum unambiguous speed.

BW = 1/(2PW) …….. (11)

Because the cycle is repeated at the same frequency as the PRF, extra copies of the main lobe will appear at various PRF intervals on each side of the carrier frequency. All the information from the return will be replayed at PRF intervals, including the Doppler-shift return. (Richards, 2005).

ISSN No: -2456-2165 https://doi.org/10.38124/ijisrt/25oct786

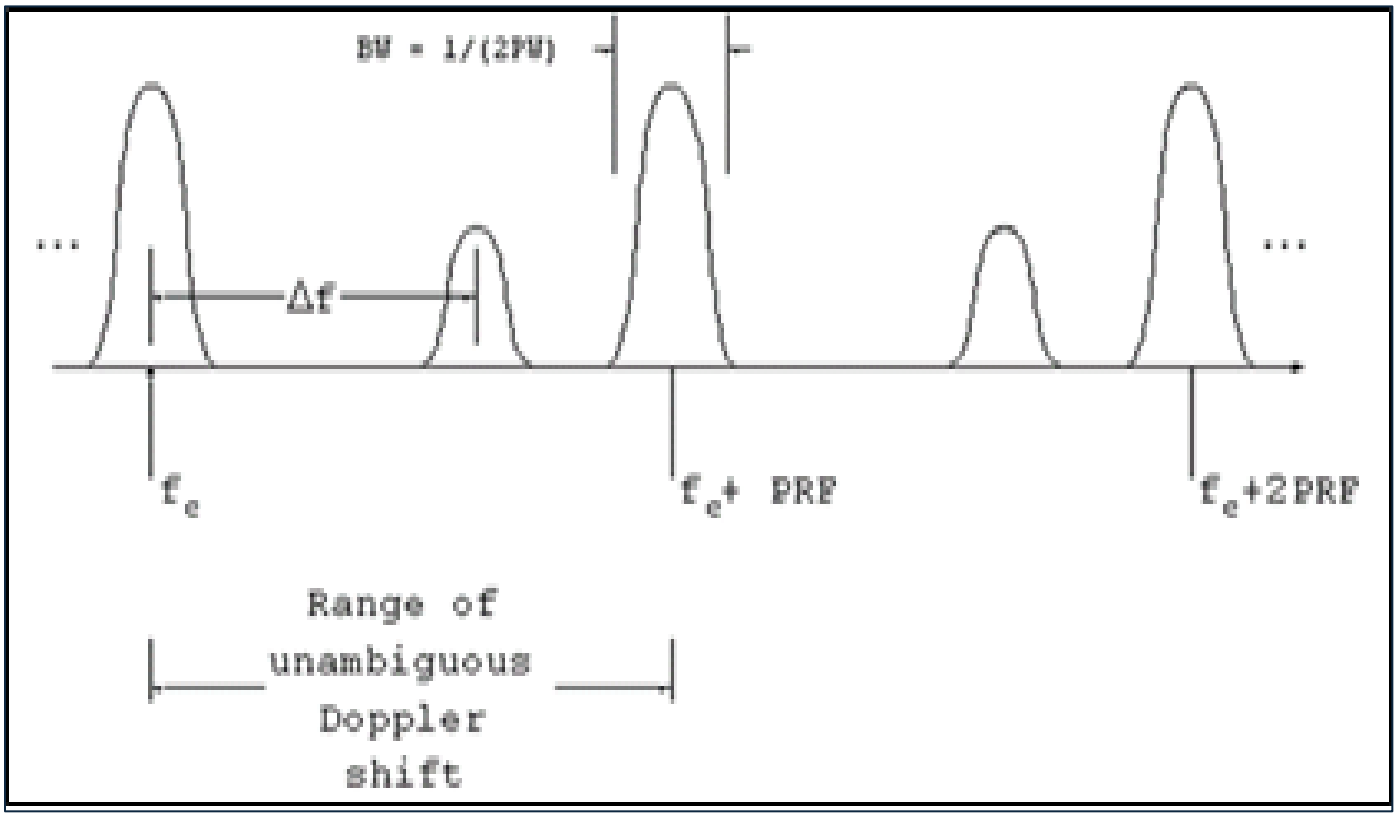

Fig 2 Spectrum of Pulsed Doppler Radar.

MTI radars exploit the variations in Doppler shifts between targets and clutter. In a phase detector, RF energy is transmitted, reflected, and combined with a reference to producing signals indicating Doppler fluctuations in moving targets. An MTI filter processes these outputs, cancelling stationary clutter pulse-by-pulse for more accurate detection.

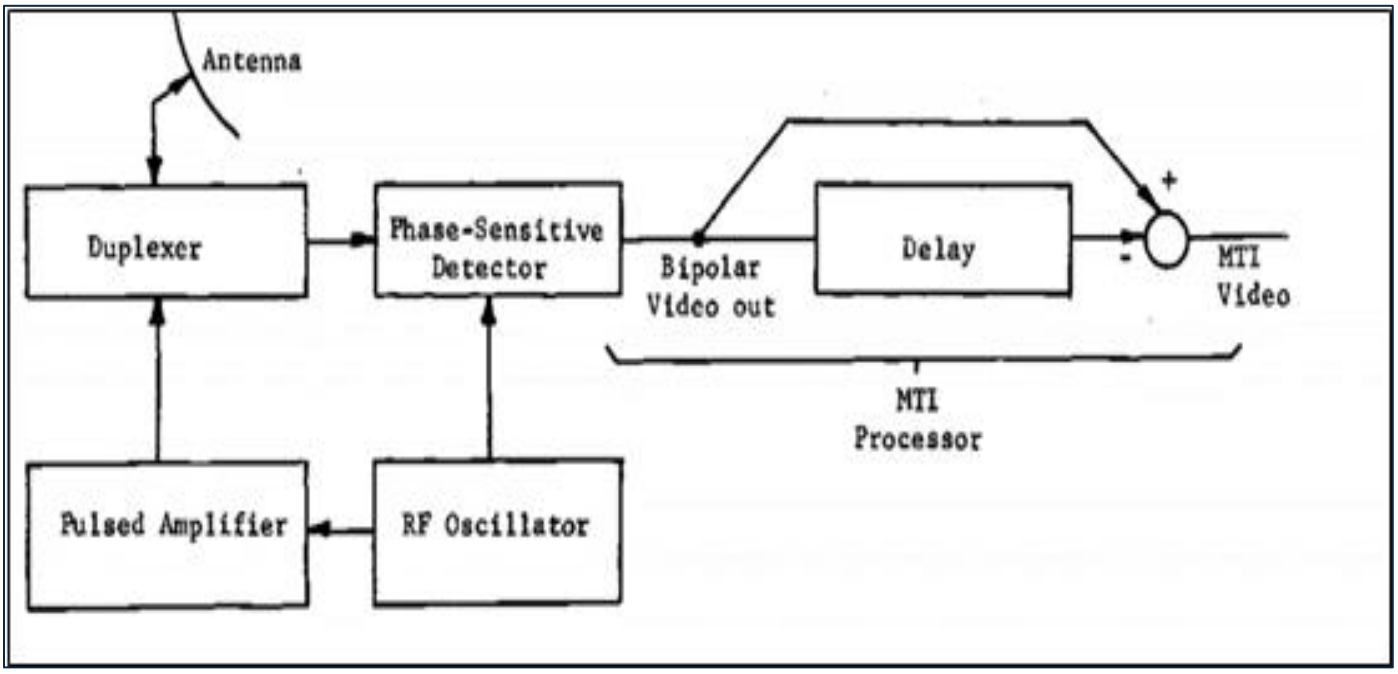

Fig 3 Simplified Block Diagram of an MTI Radar System.

MTI processors typically employ multiple received pulses to decrease clutter returns even further. In fact, higher-order cancelers are used to successfully decrease clutter by cascading more processors, as illustrated by Figure 4. The transfer function of these higher-order processors can be easily computed using z-transform techniques. Table 1 lists the transfer functions of several of these higher-order processors; for the remainder of this proposal, they will be referred to as ordinary processors. Figure 5 shows the frequency response of a standard three-pulse processor.

ISSN No: -2456-2165 https://doi.org/10.38124/ijisrt/25oct786

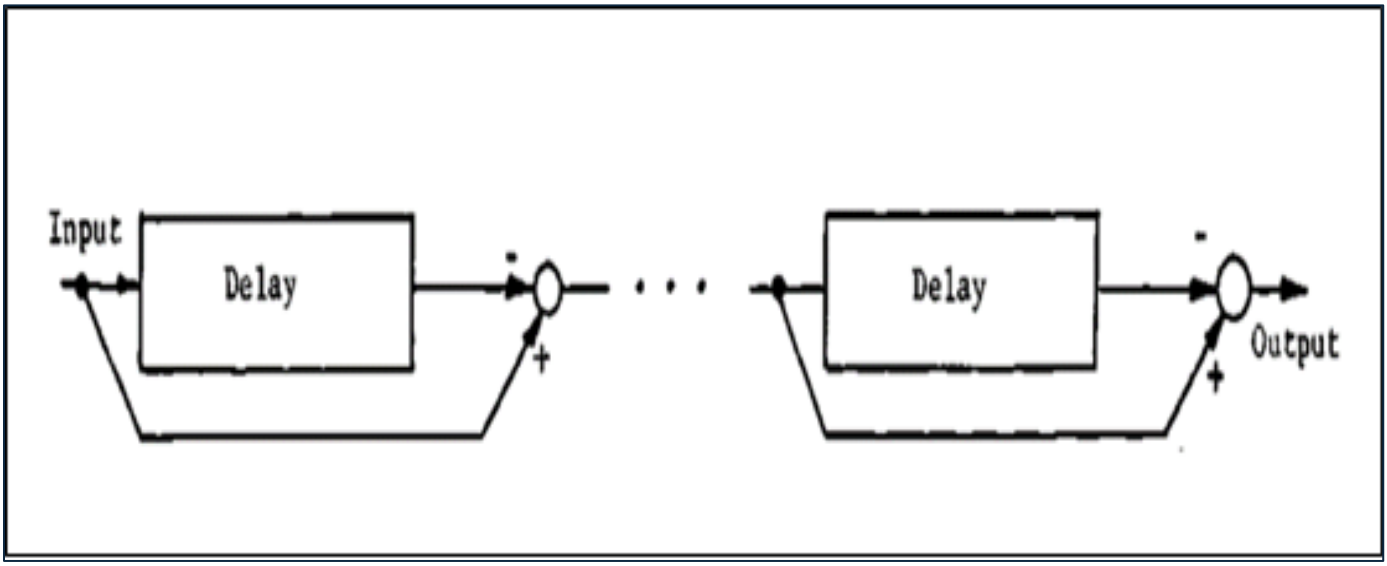

Fig 4 Two Pulse MTI Processors Yield Higher Order MTI Processors.

Table 1 Transfer Functions of Conventional MTI Processors

Number of Pulse Processed	Transfer Function (z-transform)
2	$1 - z^{-1}$
3	$1 - 2z^{-1} + z^{-2}$
4	$1 - 3z^{-1} + 3z^{-2} - z^{-3}$
5	$1 - 4z^{-1} + 6z^{-2} - 4z^{-3} + z^{-4}$

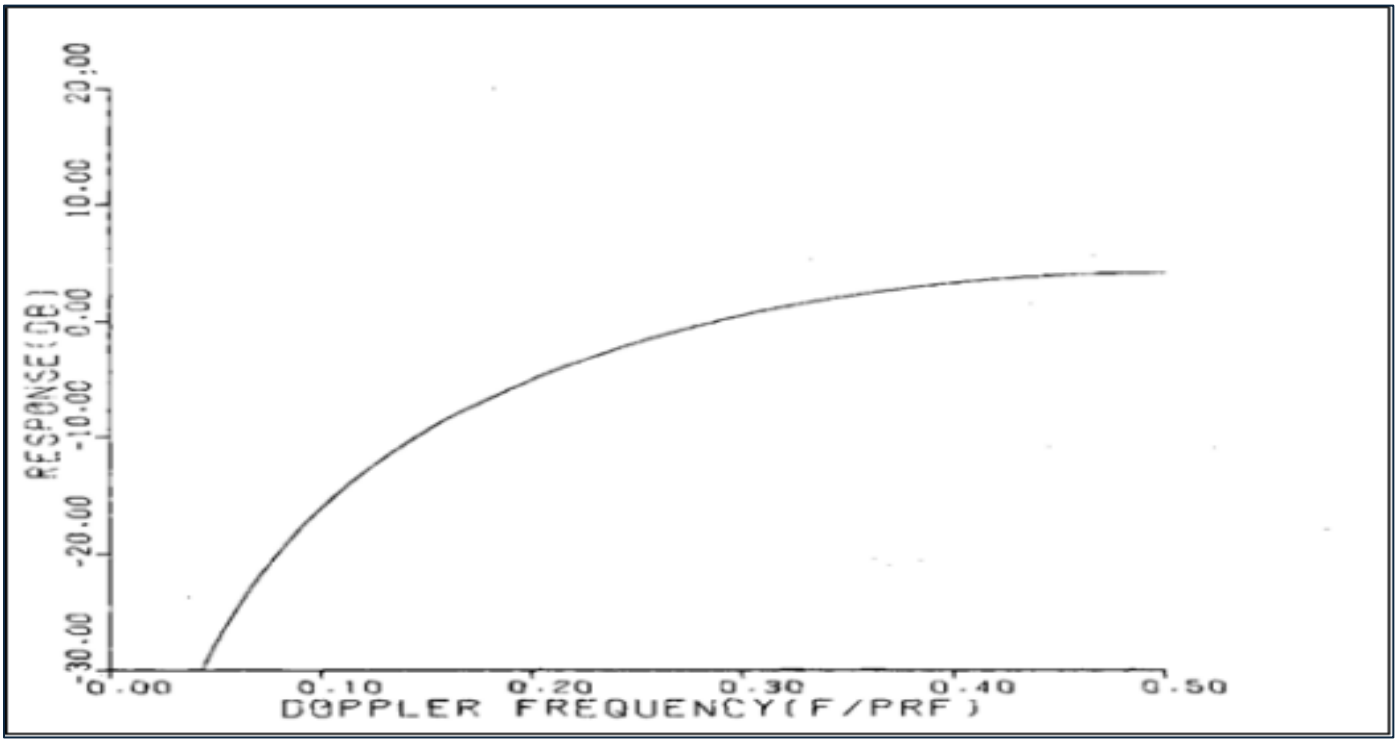

Fig 5 The Frequency Response of a Standard Three-Pulse MTI Processor. The Frequency Axis Displays the Ratio of Doppler Frequency to Pulse Repetition Frequency (PRF).

➢ *Limits on system Execution:*

MTI processors improved radar performance compared to non-MTI systems; however, their effectiveness is constrained by clutter with non-zero spectral width. Clutter from terrain, sea, or weather cannot be fully suppressed. Studies by Barlow [8], Nathanson [9], Kerr [10], Barton [11], and Skolnik [1] show clutter comprises non-fluctuating and fluctuating components, of which only the former is completely cancelable. The fluctuating component, often dominant, degrades detection. Also, clutter spectra from woodlands, oceans, and rain clouds generally follow a zero-mean Gaussian distribution. The spread of these spectra is

ISSN No: -2456-2165 https://doi.org/10.38124/ijisrt/25oct786

affected by the operating frequency, the kind of clutter, and the weather, which makes it hard to suppress. Researchers have found that the standard deviation of the clutter spectrum, which is measured in meters per second, does not depend on frequency. So, the standard deviation of the clutter spectrum, expressed in Hz, is as follows:

$$\sigma_c = \frac{2\sigma_v}{\lambda_c} \quad \text{..... (12)}$$

λ_c is the operational wavelength in meters. Scanning systems can further expand this width through scan modulation, whereas step-scan systems cannot. Table 2 summarizes some sample values for σ_c

Table 2 Summary of Standard Deviations of Clutter Spectra

Clutter Source	Wind Speed, Knots	$\sigma_v, m/sec$
Sparse Woods	Calm	0.017
Wooded Hills	10	0.04
Wooded Hills	20	0.22
Wooded Hills	25	0.12
Wooded Hills	40	0.32
Sea Echo	*	0.7
Sea Echo	*	0.75-1.0
Sea Echo	8-12	0.46-1.1
Sea Echo	Windy	0.89
Rain Clouds	*	1.8-4.0
Rain Clouds	*	2.0

Most studies adopt Gaussian spectra to describe congestion; however, Sen, S., et al. (2013] found higher frequencies in forest clutter using short-pulse, high-frequency radar. This spectrum dependency degrades system performance when processing a high number of pulses but has minimal impact on systems that handle fewer pulses. Design strategies remain adaptive, with MTI Improvement serve as a key performance indicator.

$$C = \int_{-\infty}^{\infty} C_i\,(F)d \text{ ... ...} \quad \text{(13)}$$

and the overall power at the output of the MTI processor is given by

$$C_{out} = \int_{-\infty}^{\infty} C_i\,(F)G(F)dF \quad \text{..... (14)}$$

The input time-average target-to-clutter ratio is given by $\frac{T_{in}}{C}$

$$\mathrm{r_i} = \frac{\frac{1}{2F^1}\int_{-F^1}^{F^1} \mathrm{T_{in}dF}}{\mathrm{C}} = \frac{\frac{1}{F^1}\int_{0}^{F^1} \mathrm{T_{in}dF}}{\mathrm{C}} \quad \text{..... (15)}$$

where T_{in} is the intensity of the input target signal. Taking the frequency average of the target-to-clutter ratio at the input (assuming all target velocities are equally likely).

If $\overline{T}_{in}$ is illustrated as

$$\overline{T}_{in} = \frac{1}{F^1}\int_0^{F^1} T_{in}\,dF \quad \text{..... (16)}$$

r_i might be communicated as

$$r_i = \frac{\overline{T}_{in}}{C} \quad \text{..... (17)}$$

For maximum instances of interest $T_{in} = \overline{T}_{in}$

Similarly, r_0 can be defined

$$r_0 = \frac{\frac{1}{F^1}\int_0^F T_{in}G(F)dF}{C_{out}} \quad \text{..... (18)}$$

For calculating the quantity $\overline{T}_{out}$

$$\overline{T}_{out} = \frac{1}{F^1}\int_0^{F^1} T_{in}G(F)dF \quad \text{..... (19)}$$

r_0 becomes

$$r_0 = \frac{\overline{T}_{out}}{C_{out}} \quad \text{..... (20)}$$

Then the definition of I becomes

$$\mathrm{I} = \frac{r_0}{r_i} = \frac{\overline{T}_{out}}{C_{out}} \Big/ \frac{\overline{T}_{in}}{C} = \frac{\overline{T}_{out}}{\overline{T}_{in}} \cdot \frac{C}{C_{out}} \quad \text{..... (21)}$$

using the notation,

$$\overline{T}_{in} = \frac{1}{F^1}\int_0^{F^1} T_{in}dF \quad \text{..... (22)}$$

$$\overline{T}_{out} = \frac{1}{F^1}\int_0^{F^1} T_{in}G(F)dF \quad \text{..... (23)}$$

$$C = \int_{-\infty}^{\infty} C_i\,(F)dF \quad \text{..... (24)}$$

$$C_{out} = \int_{-\infty}^{\infty} C_i\,(F)G(F)dF \quad \text{..... (25)}$$

Here,

T_{in} is the input signal power

C_i(F) is the clutter power spectral density

$G(F)$ is the power gain of the MTI processor.

ISSN No: -2456-2165 https://doi.org/10.38124/ijisrt/25oct786

$$u(t) = A(t)e^{-i(\omega_d t+\varphi_0)}+n(t) \quad \text{..... (26)}$$

$$u(t-T_r) = A(t-T_r)e^{-i(\omega_d (t-T_r)+\varphi_0)}+n(t-T_r) \quad \text{..... (27)}$$

$$R(T_r) = E[\ u(t)\, u^*(t-T_r)] = E[\ A(t)\, A(t-T_r)]e^{-i\omega_d T_r} \quad (28)$$

$$\widehat{f_d} = \frac{1}{2\pi T_r} arctan \frac{Im[\hat{R}(T_r)]}{Re[\hat{R}(T_r)]} \quad \text{..... (29)}$$

$$C(f) = P_c \frac{1}{\sqrt{2\pi}\sigma_f} exp\left[-\frac{(f-f_d)^2}{2\sigma_f^2}\right] \quad \text{..... (30)}$$

$$\begin{cases} P\{\mu-\sigma < x \le \mu+\sigma\} = \Phi(1)-\Phi(-1) = 0.6826 \\ P\{\mu-2\sigma < x \le \mu+2\sigma\} = \Phi(2)-\Phi(-2) = 0.9544 \\ P\{\mu-3\sigma < x \le \mu+3\sigma\} = \Phi(3)-\Phi(-3) = 0.9974 \end{cases}$$

III. METHODOLOGY: DIGITAL MTI PROCESSOR DESIGN AND OPTIMIZATION

➢ *Improved Digital MTI Radar Processors Design*

MTI processors are designed to meet three major requirements: achieving significant MTI improvement under heavy clutter, providing consistent target detectability across Doppler frequencies, and limiting the number of processed pulses to optimize efficiency in beam-agile or frequency-agile radars. Staggered PRF systems limit pulse spacing to maintain unambiguous range and duty cycle limits. Structured design strategies are needed to deal with these issues. We start this examination with simple, unstaggered examples of processors, such as Equal Ripple, Maximally Flat, and Constrained Improvement.

The second section discusses the design techniques for staggered PRF systems. Two kinds of processors are being worked on: maximum improvement processors (MIPs) and constraint improvement processors (CIPs). MIPs make MTI performance a lot better than older designs, while CIP design methods make processors that are more satisfying to use. These CIPs prioritize processor response consistency and accomplish the required MTI improvement value for the desired system performance. CIP designs are compared to prior ones, and exemplary CIP designs are tabulated.

➢ *Unstaggered PRF MTI Processors*

Unstaggered PRF MTI processors are special types of staggered PRF systems, which have uniform pulse spacing This enables the development of processor classes specific to unstaggered PRF. All processors here use a structured transversal filter method, with weights chosen to produce the needed MTI improvement (within quantization restrictions) while minimizing response variability when processing a set number of pulses, resulting in consistent performance.

As pointed out previously, this section looks at three types of improved processors for PRF systems that don't have staggered outputs. The first type of processor is equal ripple, the second is maximally flat, and the third is constrained improvement.

➢ *Properties of Unstaggered PRF MTI Processors*

The processor's frequency response is an extremely important attribute. Figure 6 depicts the general structure of the processor. It is clear from Figure 6 that h(t), the processor's impulse response, is provided by

$$h(t) = X_1\delta(t) + X_2\delta(t-T) + X_3\delta(t-2T) + \cdots + X_N\delta(t-(N-1)T)$$

$$\sum_{k=1}^{N} X_k\delta(t-(k-1)T) \quad \text{..... (31)}$$

where $\delta(t)$ represents a unit impulse$X_N$is the weight of the n^{th} sample, and T is the interpulse period, 1/PRF.

To compute the complex frequency response of the network, $H(\omega)$, the Fourier Transform is applied to (1), yielding

$$H(\omega) = \sum_{k=1}^{N} x_k e^{-jwT(k-1)} \quad \text{..... (32)}$$

The power response of the filter, G(ω), is then

$$\mathrm{G}(\omega) = H(\omega)H(\omega) *= C_0 + \sum_{q=1}^{n-1} C_q cos(q\omega T) \quad \text{.....} \quad (33)$$

Where,

$$C_q = \sum_{q=1}^{n-1} X_j X_{j+q} \qquad 0 \le q \le N-1 \text{ ....} \quad (34)$$

It is crucial to note that the response can be transmitted up to T = 1/PRF, and given that the Doppler frequency is expressed as F = ω/2π, the response may be communicated up to f = F/PRF. The frequency response characteristics will be examined using normalized frequency over the duration of this proposal. It facilitates the simplification of the unstaggered PRF expressions by amalgamating the weighting coefficients, the X's, to produce the Cs.

The enhancement of MTI is an additional characteristic of unstaggered PRF MTI processors, which presumes a Gaussian clutter power spectral density.

$$C_I = \frac{C}{\sigma_c\sqrt{2\pi}} e^{-F^2/2\sigma_c^2} \quad \text{..... (35)}$$

The clutter output power is given C_{out},

Where,

$$C_{out} = \int_{-\infty}^{\infty} G(F)C_I dF \quad \text{..... (36)}$$

Making the substitution $2\pi F = \omega$ in Equation 3, the above relation

Becomes

$$C_{out} = 2\int_0^{\infty}\left(C_0 + 2\sum_{q=1}^{N-1} C_q cos(2\pi F_q T)\right)\left(\frac{C}{\sigma_c\sqrt{2\pi}} e^{-F^2/2\pi_c^2}\right) dF \quad (37)$$

Or

$$C_{out} = \frac{2C}{\sigma_c\sqrt{2\pi}}\left[\int_0^{\infty} C_0 e^{-F^2/2\pi_c^2} d + 2\sum_{q=1}^{N-1}\left(C_q cos(2\pi F_q T)\right)\left(e^{-F^2/2\pi_c^2}\right)dF\right] (38)$$

ISSN No: -2456-2165 https://doi.org/10.38124/ijisrt/25oct786

And

$$C_{out} = C\left[C_0 + 2\sum_{q=1}^{N-1} C_q e^{-2q^2r^2T^2\sigma_c^2}\right] \quad \text{...(39)}$$

The average target output power, $\overline{T}_{out}$

$$\overline{T}_{out} = \frac{1}{F^1}\int_0^{F_r} \overline{T}_{in} G(F)dF \quad \text{... (40)}$$

$$= \frac{\overline{T}_{in}}{F_r}\int_0^{F_r}\left[C_0 + 2\sum_{q=1}^{N-1} C_q cos(2\pi F_q T)\right]dF$$

$$= C_0\overline{T}_{in} \quad \text{... (41)}$$

Then, substituting into the definition of improvement, one obtains

$$I = \frac{C_0}{C_0 + 2\sum_{q=1}^{N-1} C_q e^{-2q^2r^2T^2\sigma_c^2}} \quad \text{... (42)}$$

This expression checks results acquired by different authors for conventional processors, if the exponentials are extended expanded in a Taylor series and the primary non-zero terms retained. Consider the

three-pulse canceller C_0=5, C_1 =-4,C_2 =1, then

$$\frac{1}{I} = \frac{1}{5}\left[5 - 8e^{-2q^2r^2T^2\sigma_c^2} + 2e^{-2q^2r^2T^2\sigma_c^2}\right] \quad \text{... (43)}$$

Substituting,

$$e^{\alpha} \approx 1 + \alpha + \frac{\alpha^2}{2} \quad \text{... (44)}$$

$$I = \frac{f_r^4}{8\pi^4\sigma_c^4} \quad \text{... (45)}$$

which supports the conclusion provided by Nathanson [11], in which f = 1/T. The effects of clutter spectrum width can be articulated as a normalized variable σ, as indicated in Equation (4).

$$\sigma = \sigma_c T \quad \text{... (46)}$$

The utilization of this data presentation show allows an large range of PRF and σ_c to be summed up with a few carefully chosen values of σ.

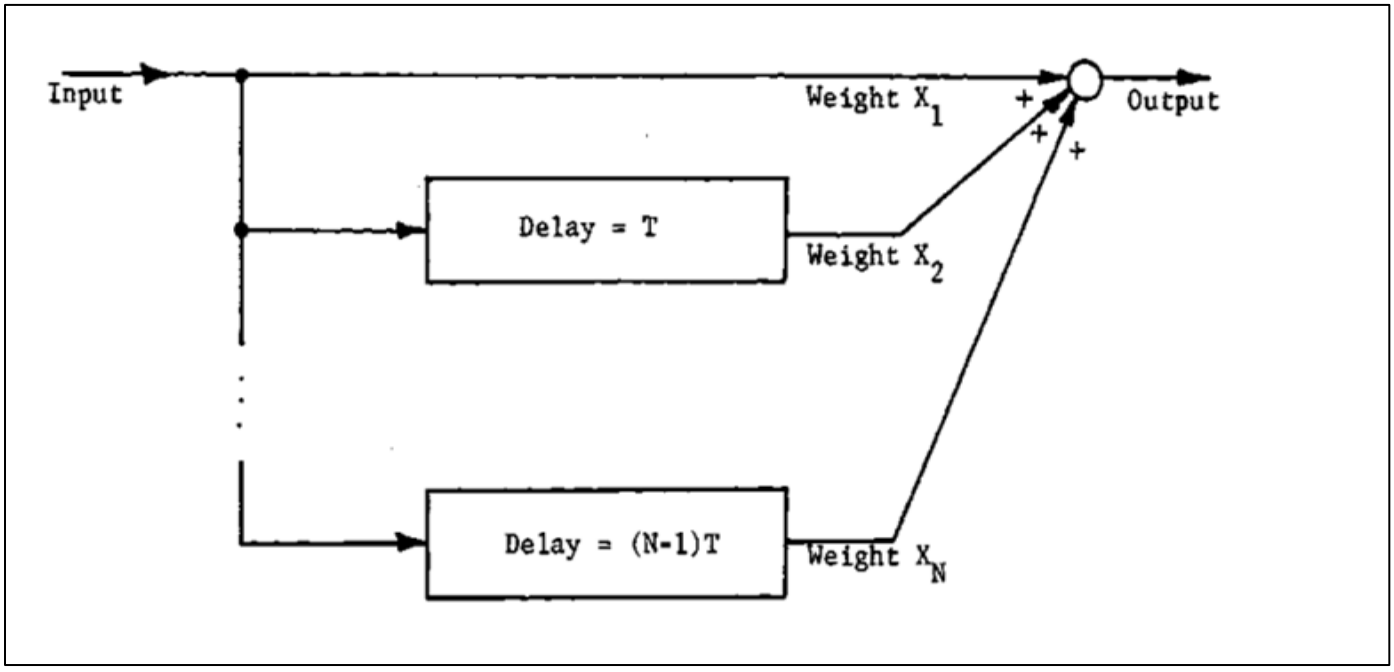

Fig 6 Equal Ripple Processors

Equal Ripple MTI processors were developed via a linear programming approach (Daellenbach & Bell, 1970) that constrained frequency response at specific intervals while optimizing a designated linear objective function. Due to the LOF, divided by I was selected for this system; to optimize the most effective filters, maximizing I necessitated a reduction in the LOF. The linear programming method utilized minimized the LOF while adhering to the set constraints on frequency response.

Designing Equal Ripple processors presented challenges, including round-off errors that impacted on the improvement factor I and the need for several equations. Despite these challenges, workable solutions were found for 3- and 5-pulse scenarios. Five-pulse processors were meant to operate between 0 and 2500 Hz, with limitations that ensured a non-negative response at zero frequency.

The ripple limitation in the passband can be set to such a stringent level that the processor offers virtually no enhancement. In Equal Ripple Processors, the ability to process a high number of pulses could have enhanced performance; however, the extensive range of available pulses ultimately constrained overall performance.

ISSN No: -2456-2165 https://doi.org/10.38124/ijisrt/25oct786

Figure 7 illustrates that when the pass band ripple limit is set to a very stringent level, the CPU provides virtually no enhancement.

Lowering the ripple constraint from 3 dB to 0.8 dB did not produce any significant attenuation at low frequencies. The required minimum frequency was established at 250 Hz.

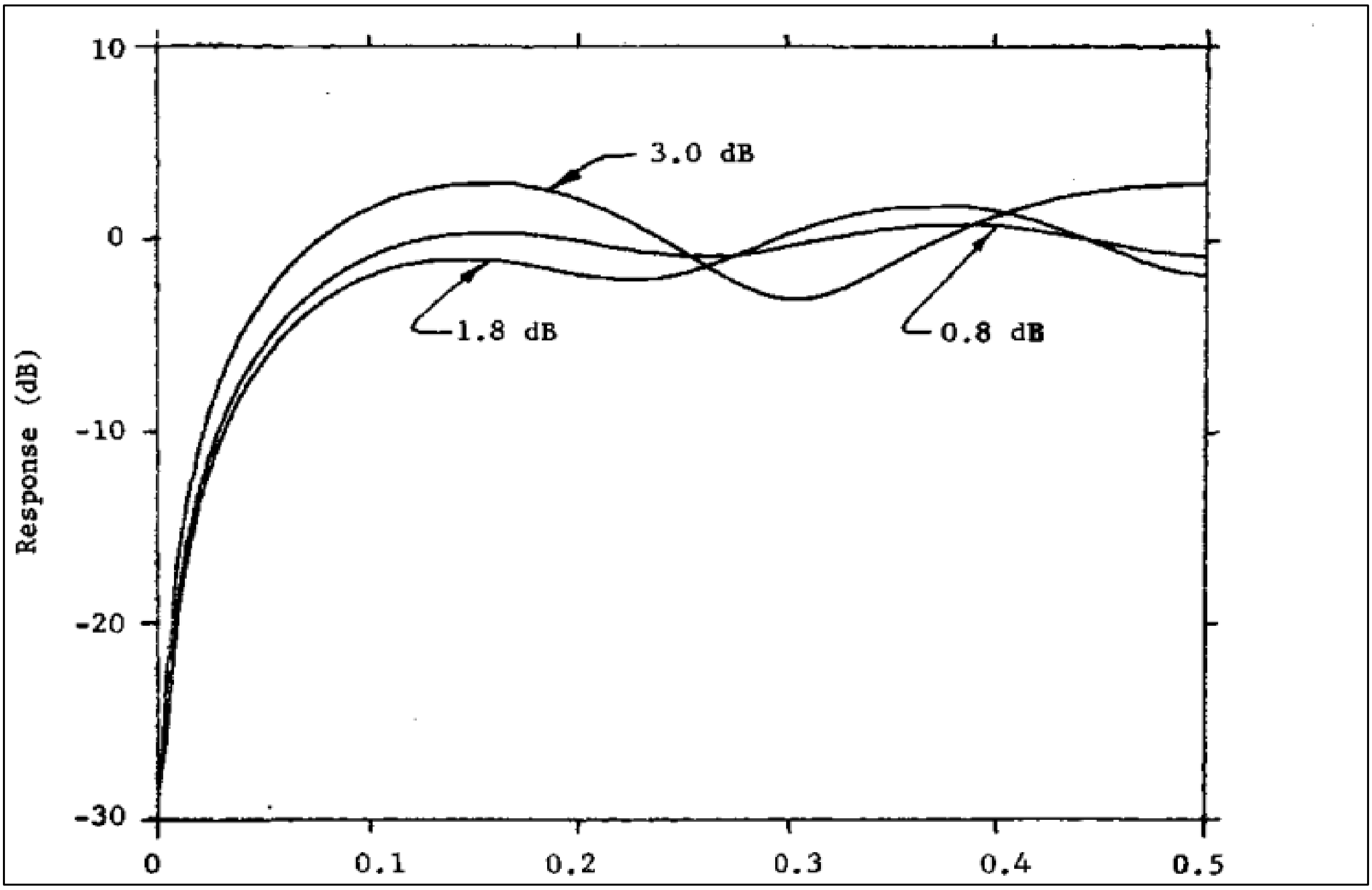

Fig 7 An Excessively Strict Ripple Specification's Effects on the Equal Ripple Processor Response.

A series of Maximally Flat Processors was developed to resolve several issues associated with Equal Ripple Processors.

The requisite MTI improvement and non-zero amplitude response are guaranteed by a Maximally Flat processor, which zeroes out selected frequency derivatives (Kuo, 2006).

This results in stable performance without trivial zero solutions.

The procedure that was employed to generate maximally flat non-recursive virtual MTI processors is as follows:

The power response of the filter is given by

$$G(\omega) = C_0 + 2\sum_{q=1}^{N-1} C_q \cos q\omega T \quad \text{...} (47)$$

and the MTI improvement, I, is given by

$$I = \frac{C_0}{C_0 + 2\sum_{q=1}^{N-1} C_q \exp(-2q^2 r^2 T^2 \sigma_c^2)} \quad \text{...} (48)$$

Going through with the above discussion, pick a value for $I = \frac{1}{Y}$, and pick out$G(\pi F_r) = 1$, where in $\omega = \pi F_r$. Following that, N-2 derivatives can be set to zero. u) = zero and/or u) = TTF were chosen as the points at which those derivatives should be set to zero. The form of the filter-out function depends on how those derivatives are distributed among various frequencies. The formulas turn into,

$$G(\pi F_r) = 1 \quad \text{...} (49)$$

$$\left.\frac{\partial G(\omega)}{\partial \omega}\right|_{\omega = \pi F_r} = 0 \quad \text{...} (50)$$

$$I = \frac{1}{Y} \quad \text{...} (51)$$

It is possible to set both derivatives of a maximally flat four-pulse processor to zero. The graphic shows the improved flatness compared to traditional processors, with the responses of three and four pulse maximally flat processors depicted.

ISSN No: -2456-2165 https://doi.org/10.38124/ijisrt/25oct786

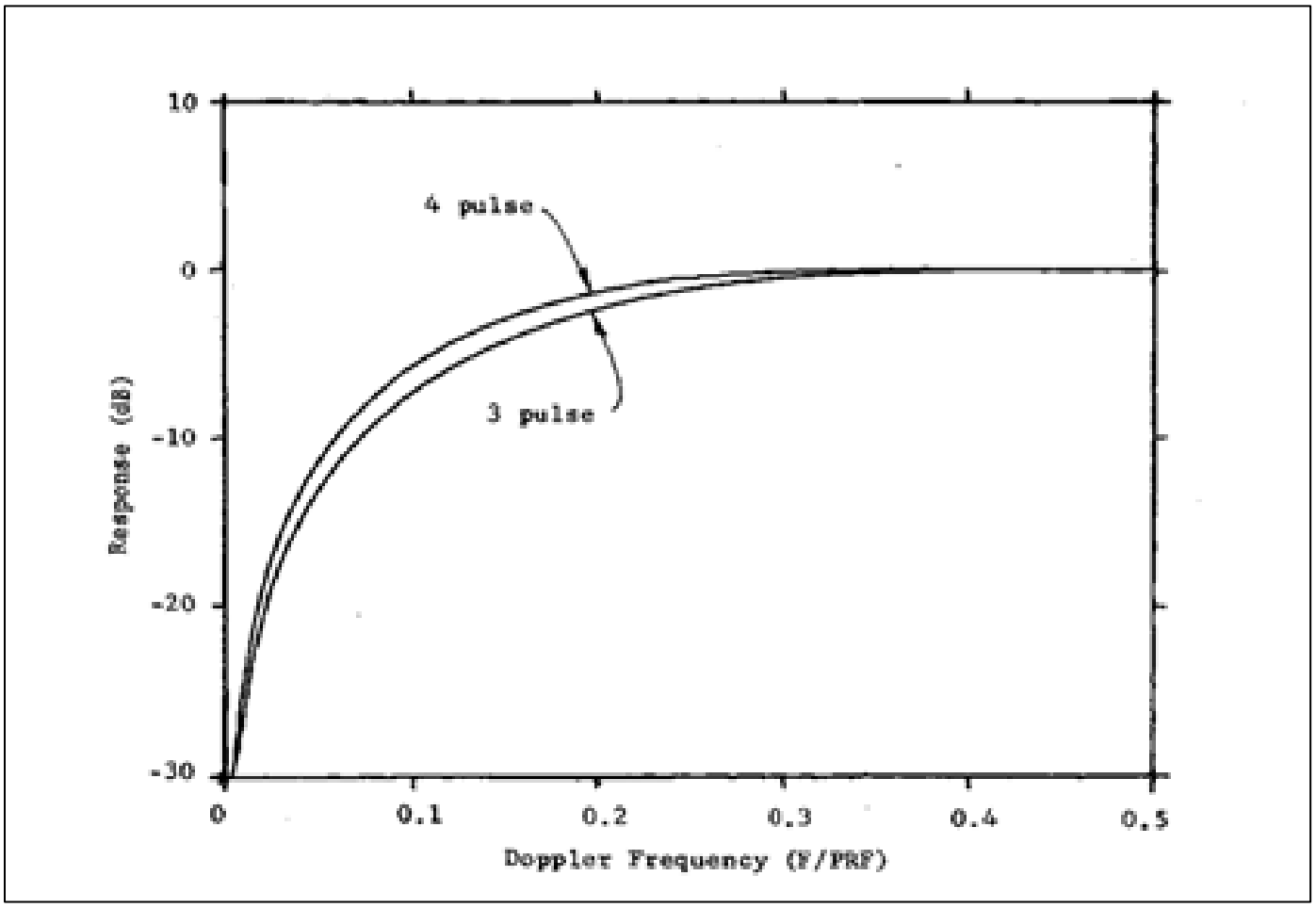

Fig 8 Maximally Flat Processor Responses for Three and Four Pulses Processed.

➢ *Constrained Improvement Processors*

Maximally Flat processors enhance uniformity at a lower computational cost than Equal Ripple designs, but they do not reduce response variation. Constrained Improvement Processors (CIPs) handle this by optimizing MTI while minimizing deviations.

$$\int_{\eta F_r}^{F_r/2}\left(G(F)-\overline{G(\bar{F})}\right)dF \quad \text{..... (52)}$$

Where,

F_r= the pulse repetition frequency,

η = a fraction $0 < \eta < 0.5$,

G(F) = the power response of the filter, and

$\overline{G(F)}$ = average response of the filter.

By selecting η, a pass band of interest is established, and the value of $\overline{G(F)}$was set to one. It is possible to use Lagrange multiplier techniques to approach this problem. Noteworthy is the fact that Martin has conducted a related analysis. He determined the integrals that resulted in Equation.

$$I = \frac{C_0}{C_0+2\sum_{q=1}^{N-1} C_q\, exp(-2q^2r^2T^2\sigma_c^2)} \quad \text{..... (53)}$$

and his analysis is a special case of the work which

follows for $\eta = 0$.

The error to be minimized over the region ηF_r to F_r /2 is the function

$$E = \int_{\eta F_r}^{F_r/2}(G(F)-1)^2 dF \quad \text{..... (54)}$$

F_r is the PRF

Substitution $\omega = 2\pi f$ in Equation (3),

$$[G(F)-1]^2 = \left[C_0 - 1 + 2\sum_{q=1}^{N-1} C_q\, cos\,(2\pi FqT)\right]^2$$

$$= (C_0-1)^2 + 4\sum_{q=1}^{N-1} C_q\, cos\,(2\pi FqT) - 4\sum_{q=1}^{N-1} C_q\, cos\,(2\pi FqT) + 4\sum_{q=1}^{N-1}\sum_{h=1}^{N-1} C_q\, C_k\, cos\,(2\pi FqT)\, cos\,(2\pi FkT) \quad \text{..... (55)}$$

ISSN No: -2456-2165 https://doi.org/10.38124/ijisrt/25oct786

Therefore,

$$E = \int_{\eta F_r}^{F_r/2} [G(F) - 1]^2 dF$$

$= (C_0 - 1)^2 (F_r/2)(1 - 2\eta) - 2C_0 \sum_{q=1}^{N-1} \sum_{h=1}^{N-1} C_q\, C_k\, F_r \alpha_{qk}$ (56)

Here,

$$\alpha_{qk} = \begin{cases} -\frac{sin2\pi\eta(q-k)}{4\pi(q-k)} - \frac{sin2\pi\eta(q+k)}{4\pi(q+k)} & q \neq k \\ \frac{1}{4}\left[1 - 2\eta - \frac{sin4\pi q\eta}{2q\pi}\right] & q = k \end{cases} \quad \ldots\ldots\ldots (57)$$

Utilizing standard LaGrange multiplier techniques, minimize

$P = E + \lambda \left(\frac{1}{I} - \gamma\right) F_r C_0$ ……………………………….. (58)

subject to the constraint that

$\frac{1}{I} = \gamma$=constant

λ is the Lagrange multiplier in these formulas. The system of equations must be solved to accomplish this.

$\frac{\partial P}{\partial C_0} = 0$ ………………………………………………… (59)

$\frac{\partial P}{\partial C_{N-1}} = 0$ ……………………………………………… (60)

$\frac{1}{I} - \gamma = 0$ ……………………………………………… (61)

Noting that $\alpha_{qk} = \alpha_{kq}$, these expressions are somewhat simplified; for

a three-pulse processor, they become

$$C_0(1 - 2\eta) - 2C_1 \frac{sin2\pi\eta}{\pi} - 2C_2 \frac{sin4\pi\eta}{\pi} + \lambda(1 - \gamma) = 1 - 2\eta - 2C_0 \frac{sin4\pi\eta}{\pi} + C_1 8\alpha_{11} + C_2 8\alpha_{22} + \lambda\left(2e^{-8\pi^2 T^2 \sigma_c^2}\right) = -2\frac{sin4\pi\eta}{2\pi} \quad (62)$$

$\begin{pmatrix} 0 \\ 1-\gamma \end{pmatrix} C_0 + C_1 2e^{-2\pi^2 T^2 \sigma_c^2} + C_2 2e^{-8\pi^2 T^2 \sigma_c^2} = 0$ ……. (63)

Ideally, processor response would be consistent across frequencies, however MTI improvement limits necessitate attenuation within the clutter spectrum. Uniformity measurements are required in order to compare non-uniform answers. A particular approach shows deviations from the desired constant behavior by computing the fraction of frequencies when responses stay within predetermined bounds and graphically representing it as a probability density function of response.

Figure 9 displays the responses of a conventional three-pulse MTI processor alongside a CIP designed for an I value of 60 dB. Targets exhibiting low-frequency Doppler returns demonstrate enhanced detectability.

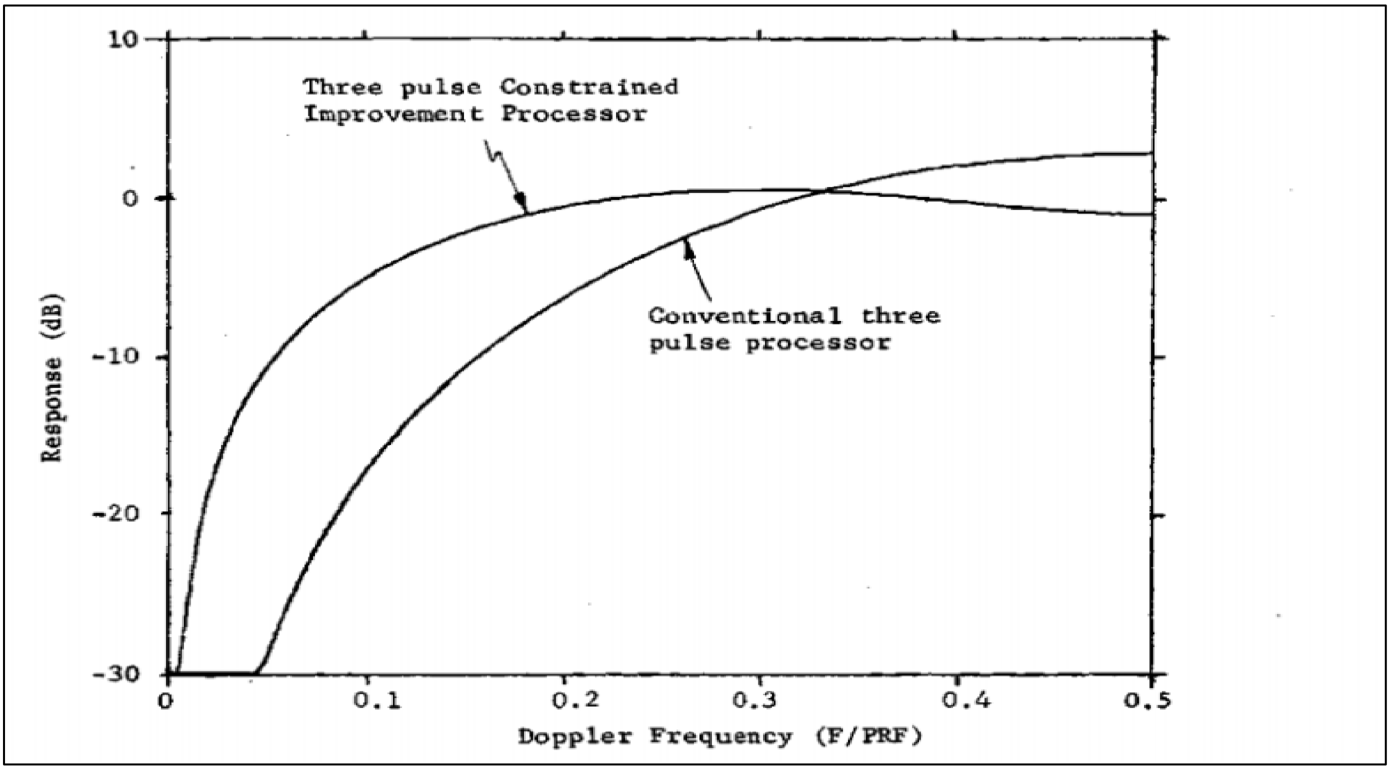

Fig 9 Comparison of the Outcomes of a Constrained Improvement Processor Designed for I = 60 dB and η = 0 with a Conventional Three Pulse Processor

ISSN No: -2456-2165 https://doi.org/10.38124/ijisrt/25oct786

The response of the single delay line canceller will be zero whenever the magnitude Sin ($\pi f_d T_p$) is zero. Which occurs when $\pi f_d T_p = 0, \pm\pi, \pm 2\pi, \pm 3\pi$

Therefore,

$$f_d = \frac{V_r}{\lambda} = \frac{n}{T_p} = nf_p, \quad n=0, 1,2, 3\ldots\ldots\ldots\ldots\ldots\ldots\ldots \quad (64)$$

Blind speeds represent a considerable limitation in MTI radar, as they result in the cancellation of specific desired moving objects with unwanted clutter at zero frequency.

- *Mitigating the Adverse Impacts of Blind Speed:*

✓ Employ a long wavelength (low frequency)
✓ Utilize a high pulse repetition frequency during radar operation.
✓ Accommodates multiple pulse repetition frequencies.
✓ Radio frequency wavelengths.

Figure 10 depicts the response of a conventional four-pulse processor to an unstaggered pulse repetition frequency system.

When radar requires Doppler frequencies exceeding the pulse repetition frequency (PRF), it is necessary to reduce blind speeds. Techniques encompass regular agility and a staggered pulse repetition frequency (PRF).

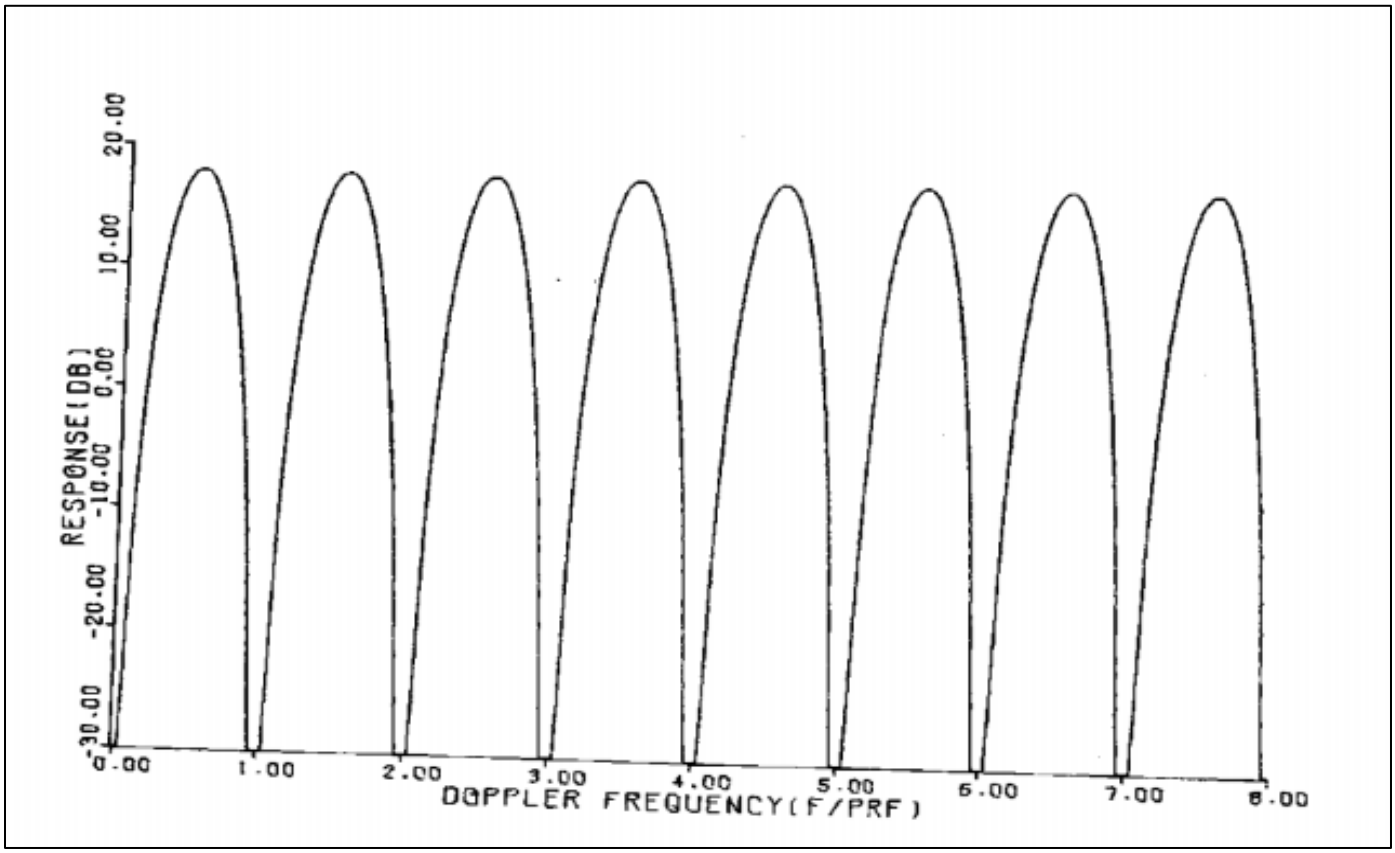

Fig 10 Response of Conventional Four Pulse MTI Processor without PRF Stagger.

➢ *Staggered PRF MTI Processors*

The staggered PRF scenario is more complicated than the unstaggered PRF case because some equations become nonlinear. Another design aspect is pulse spacing, which must be kept to precise bounds; overly narrow spacings either violate clear range requirements or exceed transmitter duty cycle constraints.

Despite these barriers, two types of modified staggered PRF MTI processors emerged: Maximum Improvement Processors (MIPs) and Constrained Improvement Processors.

MIPs are designed to enhance the MTI improvement factor (I) while maintaining a consistent average response. Its design makes use of the Fletcher-Powell algorithm and Lagrange multiplier methods to solve nonlinear equations and determine optimal filter weights for specific stagger sequences.

In contrast, CIPs specify a goal improvement factor (I) and minimize mean-square response deviations using Lagrange multipliers and Fletcher-Powell algorithms.

➢ *Properties of Staggered PRF MTI Processors*

Figure depicts the structured processor format under consideration, which shows the pulse displaced from its unstaggered position by a certain amount. Figure 11 depicts the general form of the MTI processor,

ISSN No: -2456-2165 https://doi.org/10.38124/ijisrt/25oct786

The frequency response of this processor, $H(\omega)$, is given by

$$H(\omega) = X_1 e^{-j\omega(\Delta T_1)} + X_2 e^{-j\omega(T+\Delta T_2)} + \ldots + X_N e^{-j\omega((N-1)T+\Delta T_N)}$$

$$= \sum_{i=1}^{N} X_i\, e^{-j\omega((N-1)T+\Delta T_i)} \ldots \quad (65)$$

The power response of the processor, $G(\omega)$, is given by

$$G(\omega) = H(\omega) \cdot H(\omega) * \ldots \quad (66)$$

where * denotes complex conjugate. Substituting,

$$G(\omega) = \left[\sum_{i=1}^{N} X_i\, e^{-j\omega((N-1)T+\Delta T_i)}\right] \cdot \left[\sum_{i=1}^{N} X_i\, e^{j\omega((N-1)T+\Delta T_i)}\right]$$

$$= \sum_{i=1}^{N}\sum_{j=1}^{N} X_i\, X_j \cos\left[\omega(i-j)T + \Delta T_i - \Delta T_j\right] \ldots \quad (67)$$

It is easy to simplify this notation somewhat by nothing $\omega = 2\pi F$

Here, F is the Doppler frequency, and that T = 1/PRF. Dividing the

argument of the cosine by T, one obtains

$$\sum_{i=1}^{N}\sum_{j=1}^{N} X_i\, X_j \cos\left[\frac{2\pi F}{PRE}\left((i-j) + \frac{\Delta T_i}{T} - \frac{\Delta T_j}{T}\right)\right] \ldots \quad (68)$$

Getting the substitution,

$$f = F/PRF$$

$$\Delta(i) = \Delta T_i/T$$

$$\Delta(j) = \Delta T_j/T$$

G(f) may be expressed as

$$G(f) = \sum_{i=1}^{N}\sum_{j=1}^{N} X_i\, X_j \cos\left[2\pi f\left((i-j) + \Delta(i) - \Delta(j)\right)\right] \quad (69)$$

Because of the fact that the cosine is an even function, Equation (38) may be rewritten as

$$G(f) = \sum_{i=1}^{N} X_i^2 + \sum_{k=1}^{N-1}\sum_{i=1}^{N-k} 2X_i\, X_{i+k} \cos\left(2\pi f\left(k - \Delta(i) + \Delta(i+k)\right)\right) \ldots \quad (70)$$

While Equations (5) and (6) are numerically equal, Equation (6) computes G(f) for a given set of parameters in about half the time that Equation (40) does. The average value of G(f) is $\overline{G(\bar{f})}$, providing the averaging is performed over a frequency interval significantly bigger than the PRF.

$$\overline{G(\bar{f})} = \sum_{i=1}^{N} X_i^2 \ldots \quad (71)$$

The MTI improvement, I, for the astounded PRF scenario is inferred in the same way as the unstaggered instance reviewed previously. Gaussian clutter spectrum is expected,

$$C_i = \frac{C}{\sigma\sqrt{2\pi}} e^{-f^2/2\sigma^2} \ldots \quad (72)$$

Where f=F/PRF, and $\sigma = \sigma_c T$

The clutter output power is defined by C_{out} ,

$$C_{out} = \int_{-\infty}^{\infty} G(f) C_I dF \ldots \quad (73)$$

Thus,

$$C_{out} = C\left[\sum_{i=1}^{N} X_i^2 + 2\sum_{k=1}^{N-1}\sum_{i=1}^{N-k} X_i X_{i+k} e^{-2\pi^2\sigma^2\left(k-\Delta(i)+\Delta(i+k)\right)^2}\right] \ldots \quad (74)$$

The average target output power, $\overline{T_{out}}$ is

$$\overline{T_{out}} = \frac{1}{\acute{f}} \overline{T_{in}} G(f) df \ldots \quad (75)$$

where $\acute{f}$ is the highest Doppler frequency of interest. Assuming $\acute{f}$» 1,

$$\overline{T_{out}} = \overline{T_{in}} \sum_{i=1}^{N} X_i^2 \ldots \quad (76)$$

Based on the notion of MTI improvement, I used Equations (72) and (74)),

$$I = \frac{\sum_{i=1}^{N} X_i^2}{\sum_{i=1}^{N} X_i^2 + 2\sum_{k=1}^{N-1}\sum_{i=1}^{N-k} X_i X_{i+k} e^{-2\pi^2\sigma^2\left(k-\Delta(i)+\Delta(i+k)\right)^2}} \ldots \quad (77)$$

ISSN No: -2456-2165 https://doi.org/10.38124/ijisrt/25oct786

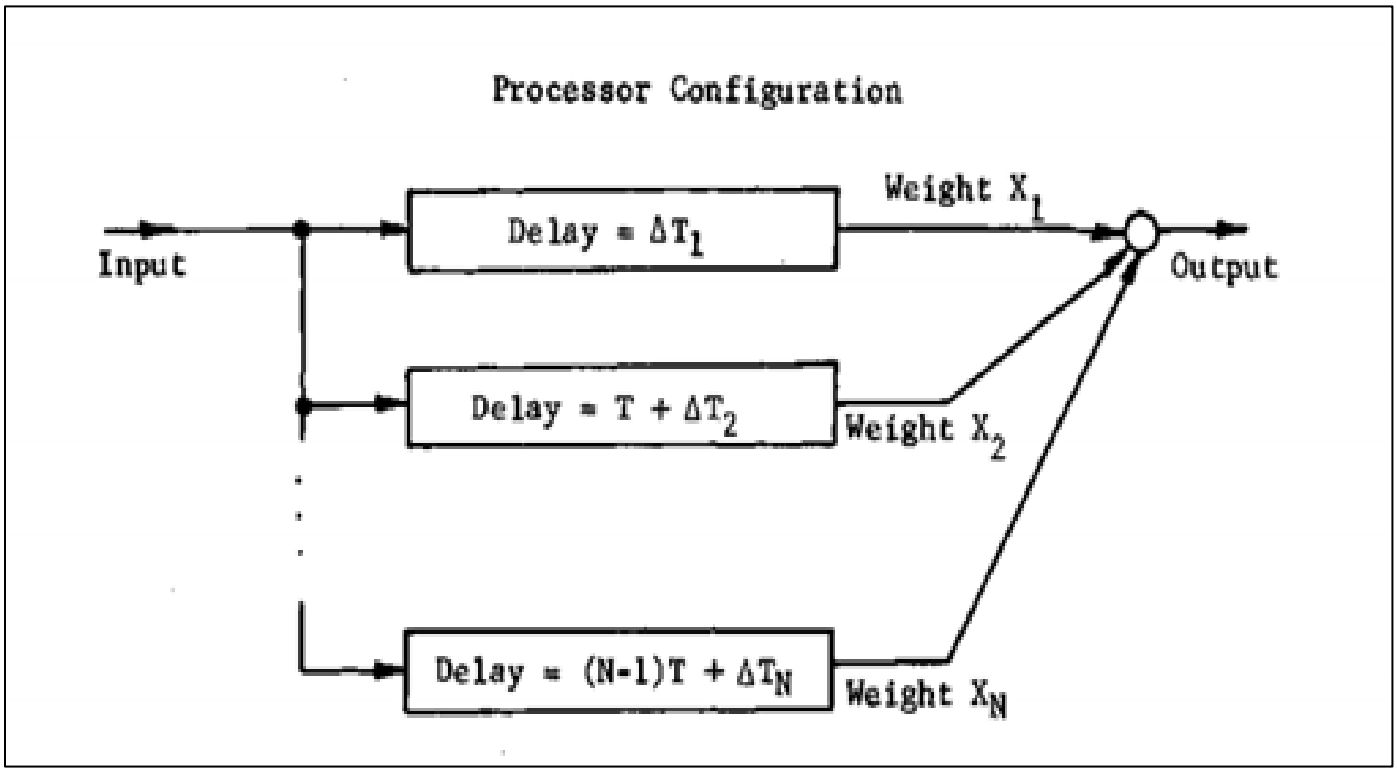

Fig 11 Pulse Stagger Sequence and Processor Configuration for Staggered PRF Processors.

IV. RESULTS AND PERFORMANCE ANALYSIS

➢ *Frequency Response of a Single Delay-Line Canceller*

A single delay-line canceler (also known as a two-pulse MTI canceler) is a high-pass filter that rejects clutter's DC component (stationary echoes at zero Doppler frequency). It removes the received signal from the previous pulse interval from the present pulse, canceling out any returns that have not changed between pulses (i.e. static clutter).

The signal from a target at range R_0 =0 at the output of the phase detector can be written

$$V_1 = (k\text{Sin}(2\pi f_d t - \varphi_0)$$

$$V_2 = k\text{Sin}(2\pi f_d (t - T_p) - \varphi_0)$$

Here,

f_d=doppler frequency shift,

R_0 =Range,

λ=wavelength,

k=amplitude of the signal

$$V = V_1 - V_2 = 2k\text{Sin}(\pi f_d T_p)\text{Cos}[2\pi f_d (t - \tfrac{T_p}{2}] - \varphi_0]$$

The frequency response function of the single delay-line canceler

$$H(f) = 2\text{Sin}(\pi f_d T_p)$$

$$H(f) = 2\text{Sin}(\pi f_d T_p)$$

This expression expresses that a single delay-line canceller completely removes clutter at 0 Doppler and cancels targets moving at blind speeds (multiples of PRF).

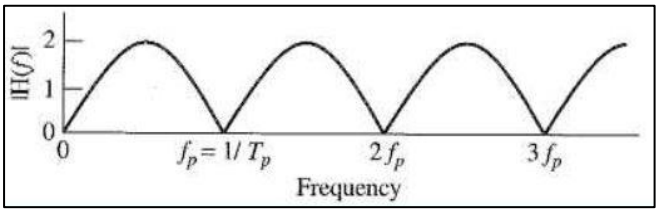

Fig 12 The Frequency Response of the Single Delay-Line Canceller

This figure illustrates the frequency response of a double delay-line canceler (a three-pulse MTI canceler) for comparison. The sinusoidal frequency response expresses alternating bands of detection and cancellation, motivating the need for higher-order filters or staggered PRFs to reduce blind speed issues. The double canceller shows greater clutter removal (a deeper stopband at zero Doppler) and a flatter pass-band between notches. The passband of the double canceller (i.e. the range of Doppler frequencies between 0 and the first blind speed) is more uniform, with less variation in gain, than that of the single canceller. This comes at the cost of expanded filter order, but it demonstrates that using more pulses (higher-order MTI filters) can enhance clutter attenuation and flatten the frequency response in the pass-band.

However, Clutter occurs not just in zero Doppler but also covers a small band of frequencies even with double or higher-order cancelers. This creates residual clutter in the passband,

ISSN No: -2456-2165 https://doi.org/10.38124/ijisrt/25oct786

especially from slow-moving objects like foliage or weather. Higher-order filters deepen the notch at zero Doppler but cannot fully eliminate distributed clutter. Besides, even blind speed targets are not detected. These problems indicate the need for adaptive filtering and staggered PRF techniques.

To confirm these theoretical attributes, we simulated frequency responses of different MTI cancelers using MATLAB. The simulations took representative radar parameters and the plot of the filter response against Doppler frequency was made. Key simulation setups and results are described below.

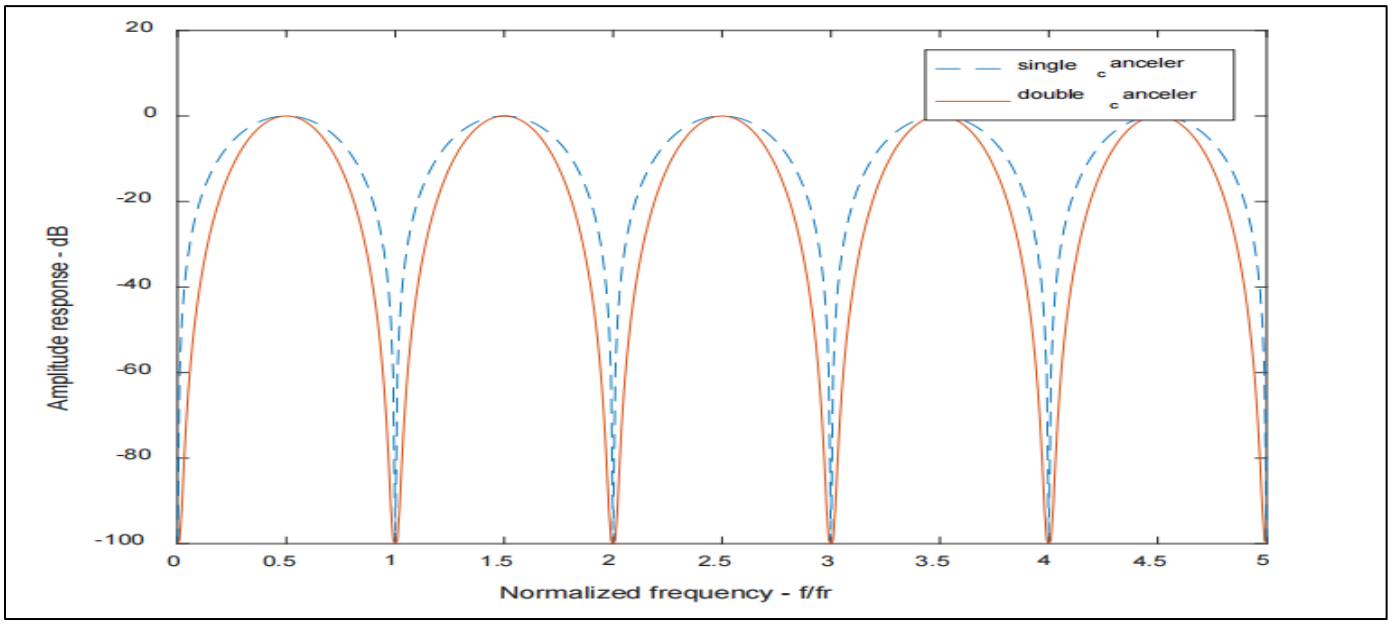

Fig 13 Normalized Frequency Response of Single Delay Line Canceller and Double Delay Line Supporter db.

We simulated the frequency responses of single and two delay-line cancellers, normalized them to the PRF, and measured the normalized responses in decibels. The generated plot contrasts their performances.

The horizontal axis indicates frequency normalized by PRF and depicts the single canceller's first blind speed at one PRF of Doppler frequency. Its response is sinusoidal, with a peak in the middle of the period and deep notches at zero and PRF multiples.

The double canceller has a similar periodicity, but with a sharper zero-Doppler notch and a flatter passband, resulting in higher clutter reduction and uniformity.

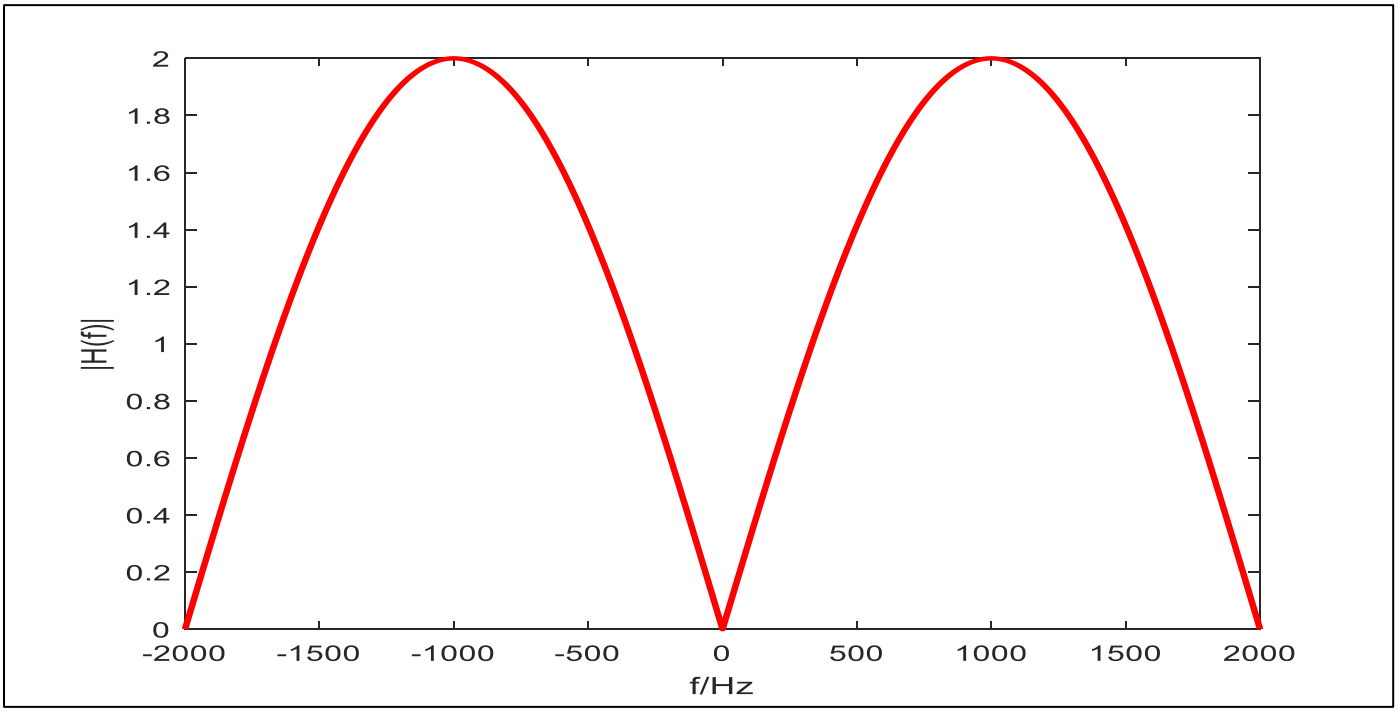

Fig 14 Frequency Response of Two-Pulse Cancellation MTI Filter

ISSN No: -2456-2165 https://doi.org/10.38124/ijisrt/25oct786

Secondly, the frequency response of the two-pulse cancellation MTI filter at a certain pulse repetition frequency was computed next. The pulse repetition frequency PRF in this simulation process has been selected as 2000 Hz, representing a pulse repetition interval, 0.0005 s. We calculated the magnitude of the filter transfer function $H(f) = 2\sin(\pi f_d T)$ across a range of Doppler frequencies (from 0 up to a few multiples of the PRF)

Figure illustrates the frequency response of a two-pulse MTI filter with a PRF fixed at 2000 Hz. The response is zero at 0 Hz and 2000 Hz, as estimated, with a peak at 1000 Hz (half PRF). The sinusoidal shape verifies simulation predictions: clutter is most reduced at zero Doppler, and maximal target amplification occurs halfway to the first blind speed. A target with Doppler at 2000 Hz is canceled, whereas one at 1000 Hz has the highest gain, exhibiting the filter's selectivity.

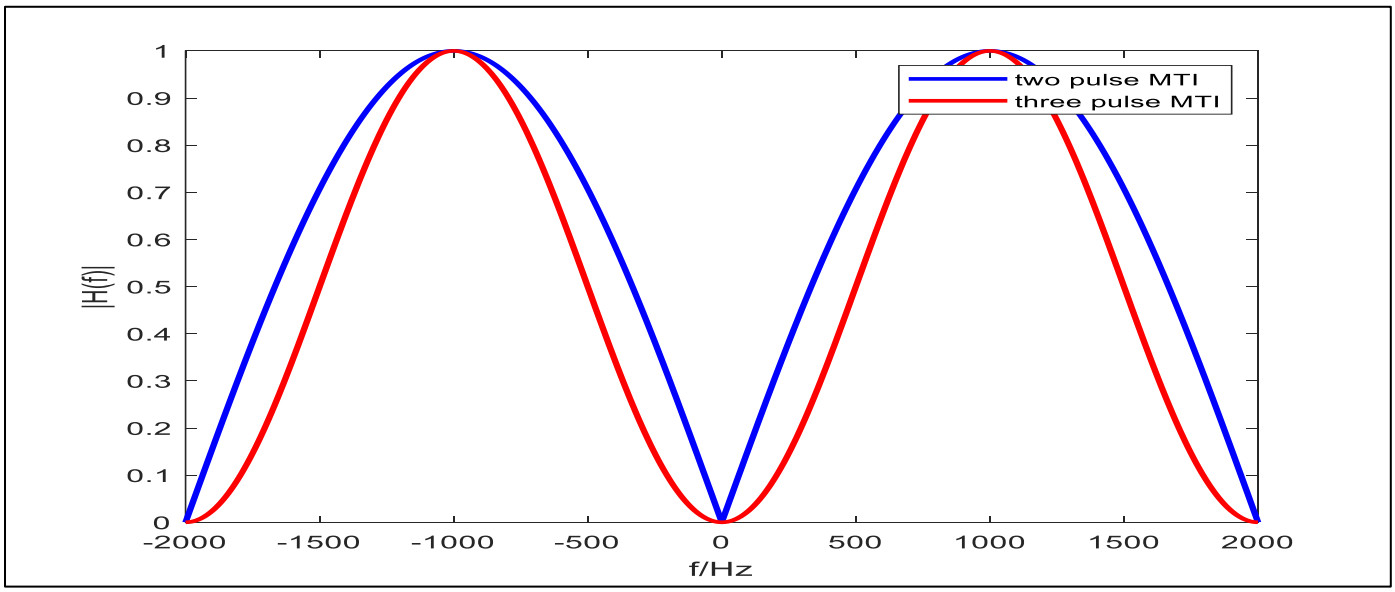

Fig 15 Frequency Response of Two-Pulse and Three-Pulse Cancellation MTI Filter

The simulation was then extended to plot two-pulse MTI filter against a three pulse MTI filter (single vs. double delay-line) on the same plot. We plotted the frequency response magnitude of the two using the same PRF of 2000 Hz.

Figure 15 exhibits the overlaid frequency responses of two- and three-pulse cancellation filters. Both responses are zero at 0 and 2000 Hz, but their forms vary dramatically between these locations.

In comparison to the two-pulse filter, the three-pulse canceller has a deeper attenuation at 0 Hz, a larger clutter notch, and a flatter passband. While the two-pulse filter has a larger mid-band gain, the three-pulse design provides more uniform clutter rejection. Both filters have the same first blind speed of 2000 Hz, but the three-pulse filter suppresses low Doppler returns more efficiently. This highlights the benefit of higher-order cancellers: larger MTI improvement factor, but at the sacrifice of passband gain and complexity.

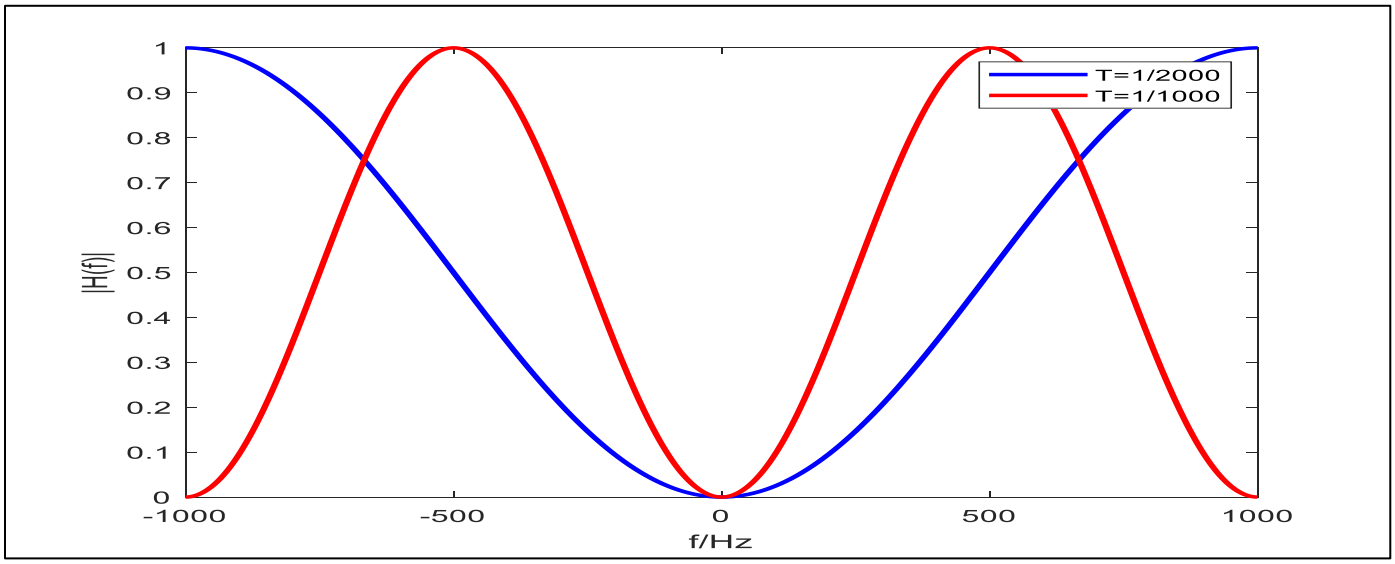

Fig 16 Frequency Response of Two MTI Filter with Different Pulse Repetition

ISSN No: -2456-2165 https://doi.org/10.38124/ijisrt/25oct786

The final simulation investigated the impact of different pulse repetition frequencies on MTI filter blind speeds. We plotted the frequency responses of two two-pulse cancellers with PRFs of 1000 and 2000 Hz. As expected, the 1000 Hz filter's first blind speed occurs at 1000 Hz Doppler, whereas the 2000 Hz filter's first notch comes at 2000 Hz.

The two responses are practically mirror-inverted: one filter has a notch, while the other has a passband peak. This complementing behavior demonstrates the benefits of staggered PRFs. By alternating PRFs across subsequent radar pulses, a target that is blind to one PRF can nevertheless be spotted by another. For example, a 1000 Hz Doppler target is undetected with a 1000 Hz PRF but easily identifiable with a 2000 Hz PRF, and vice versa. Thus, using staggered PRFs, the blind zones of one filter are covered by the detectable range of the other, resulting in robust detection.

Overall, these results illustrate the practical utility of staggered PRF in modern MTI radar, where such sequences are commonly utilized to avoid target loss at specified velocities. Overall, the MATLAB simulations confirm theory, demonstrating periodic Doppler nulls, greater clutter suppression with higher-order filters, and the efficiency of PRF variation in reducing blind speeds.

V. CONCLUSION AND FUTURE SCOPE

This study has shown how Moving Target Indication (MTI) radar processors could be designed, analyzed, and performance evaluated, with particular attention to overcoming the fundamental limitations of traditional designs. The two-pulse or three-pulse cancellers are effective as traditional MTI processors but have several shortcomings: non-uniform frequency response across Doppler frequencies, large variations in target detectability, blind speed effects, and large numbers of pulses are needed to have a significant effect on clutter suppression. All these problems reduce the capability of the previous systems to deliver reliable detection at realistic radar conditions, where dynamic sources of clutter are present, such as wind-blown vegetation, sea clutter, or weather returns.

To overcome these deficiencies, the study was directed at coming up with optimized processor designs that will guarantee sufficient clutter suppression as well as consistency in response throughout the Doppler spectrum. Three major types of processors were investigated in the unstaggered PRF case., which employs linear programming to balance frequency response ripple against improvement factor; the Maximally Flat Processor, which achieves smooth responses by forcing higher-order derivatives of the transfer function to vanish at selected frequencies; and the Constrained Improvement Processor (CIP), which sets a target MTI improvement factor while minimizing response variation using Equal Ripple Processor Lagrange multiplier techniques. Each of these designs provides a unique tradeoff between the complexity of implementation, stability of response, and the degree of improvement achievable, but all designs achieve a better balance of consistency of performance in detecting moving targets than conventional cancellers.

For staggered PRF systems, where pulse spacings vary to avoid blind speed overlap, two advanced processor classes were considered: the Maximum Improvement Processor (MIP), designed to maximize the MTI improvement factor subject to average response constraints, and the Constrained Improvement Processor (CIP) adapted for staggered PRFs, which ensures a desired level of improvement while reducing mean-square response deviations. Staggered designs, though mathematically more challenging and thus necessitating nonlinear optimization tools like Fletcher Powell algorithms, are potent in enhancing coverage of the target by eradicating the blind speed and enhancing the clutter rejection within a broader doppler range.

The developments were confirmed using MATLAB simulations of the frequency responses. It was found that the higher order cancellers offer a deeper notch at the zero Doppler and flatter passbands, which is the result that offers better clutter and more even detectable features. Moreover, comparative simulations between the PRF and other PRFs helped demonstrate that staggered PRF can effectively remove blind speeds: objects that cannot be detected at a specific PRF are visible when the radar is switched to another. These results support the usefulness of staggered PRF designs in combination with state-of-the-art processors.

Overall, the research establishes that modern digital MTI processors can be designed to achieve both the required improvement factor and stability of response, leveraging optimization methods and adaptive filter design. This has been combined with the better processor structures and staggered PRF operation to offer substantial performance improvement over traditional MTI systems. They are more effective suppression of stationery and slow-moving clutter, removal of blind speed gaps and the consistent detection of targets at a large range of velocities. These developments are essential in the current radar systems, where digital signal processing resources permit elaborate filter implementations. The results of this research not only support the theoretical knowledge of MTI radar processing but also provide practical principles of creating an efficient clutter rejection system in advanced defense, weather surveillance and monitoring, and surveillance practice

REFERENCES

[1]. Barton, D. K., & Ward, H. R. (1969). Handbook of Radar Measurement. Prentice Hall.
[2]. Cho, S., Lee, J. Y., & Han, J. (2025). Adaptive Sea Clutter Suppression for Marine Radar Systems to Enhance Uncrewed Surface Vehicle Autonomy. *NAVIGATION: Journal of the Institute of Navigation*, *72*(1), navi.687. https://doi.org/10.33012/navi.687
[3]. Daellenbach, H. G., & Bell, E. J. (1970). *User's Guide to Linear Programming*. Prentice Hall.
[4]. Galati, G., Pavan, G., & Wasserzier, C. (2022). Signal design and processing for noise radar. *EURASIP*

ISSN No: -2456-2165 https://doi.org/10.38124/ijisrt/25oct786

Journal on Advances in Signal Processing, *2022*(1). https://doi.org/10.1186/s13634-022-00884-1

[5]. Gini, F. (2021). Grand Challenges in Radar Signal Processing. *Frontiers in Signal Processing*, *1*. https://doi.org/10.3389/frsip.2021.664232

[6]. Griffiths, L., & Rude, M. (2005). Adaptive filtering without a desired signal. https://doi.org/10.1109/icassp.1987.1169735

[7]. Jing, X., Su, H., Shen, L., Mao, Z., & Jia, C. (2023). Adaptive Radar Detection in the Clutter and Noise Cover Pulse Jamming Environment. Signal Processing,205,108852. https://doi.org/10.1016/j.sigpro.2022.108852

[8]. Kerr, D. E. (1965). *Propagation of Short Radio Waves*

[9]. Klemm, R., & Institution Of Engineering And Technology. (2006). *Principles of space-time adaptive processing*. Institution Of Engineering And Technology.

[10]. Kuo, F. (2006). *NETWORK ANALYSIS AND SYNTHESIS, 2ND ED*. John Wiley & Sons.

[11]. Nathanson, F. E. (1969). *Radar Design Principles*. McGraw-Hill Companies.

[12]. Riabukha, V. P., Semeniaka, A. V., Katiushyn, Y. A., & Atamanskiy, D. V. (2022). Comparative Experimental Investigations of Adaptive and Non-adaptive MTI Systems in Pulse Radars of Various Applications and Wave Ranges. *Radioelectronics and Communications Systems*, *65*(4), 165–176. https://doi.org/10.3103/s073527272204001x

[13]. Richards, M. A. (2005). *Fundamentals of Radar Signal Processing*. McGraw Hill Professional.

[14]. Skolnik, M. I. (2008). Radar handbook. Mcgraw-Hill.

[15]. Tan, L., & Jiang, J. (2025). Digital Signal Processing. Elsevier.

[16]. Vaidyanathan, P. P. (1990). Multirate digital filters, filter banks, polyphase networks, and applications: a tutorial. *Proceedings of the IEEE*, *78*(1), 56–93. https://doi.org/10.1109/5.52200

[17]. Van, H. L. (2001). *Detection, estimation and modulation theory. Part 1*. John Wiley & Sons Inc.

[18]. Ward, E., Shahzad Gishkori, & Mulgrew, B. (2021). Compressive Sensing Technique for Mitigating Nonlinear Memory Effects in Radar Receivers. *IEEE Transactions on Aerospace and Electronic Systems*, *58*(2), 1005–1020. https://doi.org/10.1109/taes.2021.3112116

[19]. Xu, L., Sun, S., Zhang, Y. D., & Petropulu, A. P. (2024). Reconfigurable Beamforming for Automotive Radar Sensing and Communication: A Deep Reinforcement Learning Approach. *Deleted Journal*, *1*, 124–138. https://doi.org/10.1109/jsas.2024.3431462

[20]. You, H., Xiu Jianjuan, & Xin, G. (2016). *Radar Data Processing With Applications*. John Wiley & Sons.

[21]. *Yuan, B.H., Zhang, W.X. and Zhong, X.K. (2017) Reconfigurable Multi-Channel Radar Transmitter Based on SDR. Applied Science and Technolo-gy. - References - Scientific Research Publishing*. (2017). Scirp.org. https://www.scirp.org/reference/referencespapers?referenceid=2096635

[22]. Zhang, R., Xue, J., & Zhang, T. (2025). Reliable Clutter Suppression for Slow-Moving Weak Target Radar Detection. *2022 IEEE International Conference on Communications Workshops (ICC Workshops)*, 354–359. https://doi.org/10.1109/iccworkshops67674.2025.11162253